PHOTONICS Research

Observation of optical refrigeration in a holmium-doped crystal

Saeid Rostami, Alexander R. Albrecht, Azzurra Volpi, and Mansoor Sheik-Bahae*

Department of Physics and Astronomy, University of New Mexico, Albuquerque, New Mexico 87131, USA
**Corresponding author: msb@unm.edu*

Received 19 November 2018; revised 31 January 2019; accepted 15 February 2019; posted 15 February 2019 (Doc. ID 352278); published 18 March 2019

We report, to the best of our knowledge, the first demonstration of solid-state optical refrigeration of a Ho-doped material. A 1 mol% Ho-doped yttrium lithium fluoride (YLF) crystal is cooled by mid-IR laser radiation, and its external quantum efficiency and parasitic background absorption are evaluated. Using detailed temperature-dependent spectroscopic analysis, the minimum achievable temperature of a 1% Ho:YLF sample is estimated. Owing to its narrower ground- and excited-state manifolds, larger absorption cross section, and the coincidence of the optimum cooling wavelength of 2070 nm with commercially available high-power and highly efficient Tm-fiber lasers, Ho^{3+}-doped crystals are superior to Tm^{3+}-doped systems for mid-IR optical refrigeration. With further improvement in material purity and increased doping concentration, they offer great potential towards enhancing the cooling efficiency nearly two-fold over the best current Yb:YLF systems, achieving lower temperatures as well as for the realization of eye-safe mid-IR high-power radiation balanced lasers.

https://doi.org/10.1364/PRJ.7.000445

1. INTRODUCTION

Optical refrigeration relies on anti-Stokes fluorescence [1] where absorption of low-entropy and coherent light (i.e., laser) with photon energy $h\nu$ is followed by efficient emission of high-entropy spontaneous emission (fluorescence) with a mean energy of $h\nu_f > h\nu$, as shown schematically in Fig. 1(a). This excess energy in fluorescence must be extracted from the internal energy of the system (e.g., phonons), thus leading to net cooling. The optical cooling efficiency η_c, defined as the heat-lift per absorbed photon, is expressed as [2]

$$\eta_c = p\frac{h\nu_f}{h\nu} - 1, \tag{1}$$

where $p \lesssim 1$ denotes the probability that an absorbed pump photon will lead to a fluorescence photon exiting the system. According to Eq. (1), a large detuning of the pump laser energy $h\nu$ from mean fluorescence energy $h\nu_f$ is favorable to achieve higher cooling efficiencies; however, a sharp drop in the resonant absorption coefficient at large-red-detuning from $h\nu_f$ effectively sets a practical limit on pump detuning to $h\nu_f - h\nu \sim O(kT)$, which in turn entails $p > 1 - kT/h\nu \sim 98\%$, assuming ~1 eV transition at room temperature.

In 1950, Kastler [3] proposed rare-earth (RE)-doped solids as suitable candidates for fluorescence cooling due to their extremely high fluorescence efficiency. The first observation of optical refrigeration, however, did not materialize until 1995, when researchers at Los Alamos National Laboratory reported net cooling of a high-purity Yb-doped ZBLANP glass [4] at a laser wavelength $\lambda = 1030$ nm. Since then, considerable advances [5–8] have been made towards achieving cryogenic operation by exploiting high-purity crystalline host materials such as $YLiF_4$ (YLF) [9,10]. Most recently, a Yb:YLF crystal was cooled to below 90 K from room temperature [11]. Another major milestone in optical refrigeration reported this year involved the long-awaited tangible application of this technology: an arbitrary load (in this case, a HgCdTe IR sensor) was cooled to 135 K, which marked the first realization of an all-solid-state cryogenic refrigerator device with a universal cold finger [12]. Such cryocoolers offer certain advantages over their existing mechanical counterparts, as they are virtually vibration free and can have superior reliability and lifetime, due to their lack of moving parts. Currently, a drawback of this technology is its rather low efficiency (<1%). This limitation, however, is not a fundamental one: it has been suggested that with larger detuning (in extremely high-purity crystals) and/or fluorescence harvesting (e.g., using photovoltaic convertors [13] or Stokes shifters [14]), this is limited only by the Carnot efficiency [14]. An obvious alternative to enhance the efficiency is to use lower energy transitions. This becomes apparent by rewriting Eq. (1) assuming $p \sim 1$ and a detuning of $\sim kT$, which gives $\eta_c \approx kT/h\nu$, signifying an inverse scaling of cooling efficiency with photon energy. This scaling law was first validated by cooling 1% Tm:ZBLANP glass at $\lambda \sim 2000$ nm, thus improving the efficiency nearly two-fold over Yb-doped systems [15]. Later in mid-IR, Tm^{3+}:BaY_2F_8 (Tm:BYF)

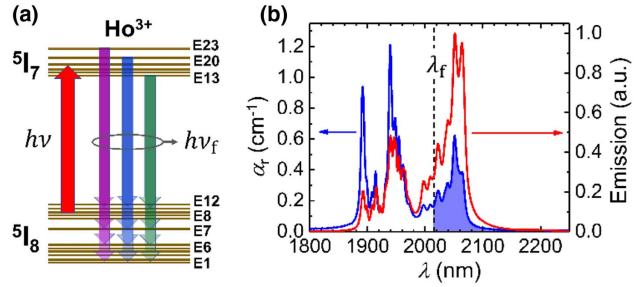

Fig. 1. (a) Anti-Stokes fluorescence cooling process in Ho^{3+} ions; (b) emission (red line) and absorption (blue line) spectra of 1% Ho:YLF crystal at $T = 300$ K ($\lambda = c/\nu$). The shaded region denotes the cooling tail ($\lambda > \lambda_f = 2015$ nm). Emission spectrum is measured with a scanning optical spectrum analyzer under laser excitation at 1890 nm. The absorption spectrum is directly measured with an FTIR spectrometer under $E \| c$ configuration (c is the optical axis).

crystals were also cooled successfully with improved performance [16]. Attempts to cool Ho-doped chloride and bromide crystals in mid-IR were unsuccessful, possibly due to OH-absorption [17].

Another advantage of mid-IR optical refrigeration is material purity. Based on Yb cooling results [18], the current assumption is that the major contamination is caused by transition metals (e.g., iron [19]), which have much smaller absorption cross sections in the mid-IR compared to the near-IR [20].

A figure of merit for any cooling-grade material is its so-called minimum achievable temperature (MAT). This quantity is defined by the lowest temperature at which η_c vanishes and subsequently turns negative (i.e., enters the heating regime). MAT is not a fundamental property of a dopant or host; rather, it is highly sensitive to the growth quality and purity of any given material. This further becomes apparent by examining the constituents of η_c, namely, ν_f and p, and their variation with temperature. It is straightforward to show that deviation of p from unity is due to the ubiquitous presence of both nonradiative decay and unwanted impurities that cause parasitic heating, i.e., $p(\nu, T) = \eta_{\text{ext}}\eta_{\text{abs}}(\nu, T)$, where $\eta_{\text{ext}} = (1 + W_{nr}/\eta_e W_r)^{-1}$ is the external quantum efficiency (EQE) and $\eta_{\text{abs}}(\nu, T) = [1 + \alpha_b/\alpha_r(\nu, T)]^{-1}$ denotes the absorption efficiency [2,14]. Here, W_r, W_{nr}, α_b, and $\alpha_r(\nu, T)$ are radiative and nonradiative decay rates, background, and resonant absorption coefficients, respectively. Additionally, the radiative (spontaneous emission) rate is effectively suppressed by the fluorescence escape efficiency η_e, which takes into account the effect of fluorescence reabsorption as well as radiation trapping via total internal reflection. It is quite reasonable to assume that η_{ext} is only weakly temperature dependent. The overriding temperature dependence of $p(\nu, T)$ arises from $\alpha_r(\nu, T)$ for wavelengths near the optimum cooling efficiency, corresponding to transitions originating from the top of the ground state. Under the plausible assumption that Boltzmann quasi-equilibrium establishes in each manifold prior to spontaneous emission, this temperature dependence follows $\alpha_r(\nu, T) \propto (1 + e^{\delta E_{\text{gs}}/kT})^{-1}$, where δE_{gs} is the width of the ground-state manifold [14]. Similarly, with Boltzmann quasi-equilibrium established in the excited-state manifold, the mean fluorescence energy red shifts as the temperature of the crystal is lowered according to $h\nu_f(T) \sim h\nu_f(0) + \delta E_{\text{es}}/(1 + e^{\delta E_{\text{es}}/kT})$, where δE_{es} denotes the width of the excited-state manifold [14]. Such functional dependences on the widths of energy manifolds are indeed the key factors that have rendered YLF a suitable host material for optical refrigeration due to its rather weak Stark crystal field acting on RE dopant ions. Similarly, the main motivation of investigating Ho^{3+} is the fact that it has narrower ground- and excited-state manifolds ($\delta E_{\text{gs}} = 303$ cm^{-1}, $\delta E_{\text{es}} = 140$ cm^{-1}) compared to Tm^{3+} ($\delta E_{\text{gs}} = 419$ cm^{-1}, $\delta E_{\text{es}} = 373$ cm^{-1}) for a given host [21]. It is also worth noting that the manifolds in Ho^{3+} are narrower than those in Yb^{3+} (YLF) [22], with $\delta E_{\text{gs}} = 449$ cm^{-1} and $\delta E_{\text{es}} = 278$ cm^{-1}, providing further advantage of Ho for cryogenic refrigeration. In the following, we describe experimental details of laser cooling of a 1% Ho:YLF crystal; this represents the first observation of laser cooling of any Ho-doped solid. We will discuss the prospects of a Ho-doped crystal for cryogenic cooling and the necessary conditions to obtain higher cooling efficiency than in Yb-based systems, as well as its potential for mid-IR radiation balanced lasers.

2. RESULTS: ROOM-TEMPERATURE ANALYSIS

RE-doped fluoride single crystals with the exquisite high purity and structural quality required for laser cooling applications are not readily available commercially. The 4.8 mm × 4.8 mm × 5.0 mm 1% Ho:YLF crystal investigated in this work was grown by the Czochralski process at AC Materials (Tarpon Springs, Florida), one of the few providers of sufficiently high-quality fluoride crystals currently available worldwide. High-purity (5N for REs with minimal concentrations of transition metals) binary fluorides were used as starting materials for the growth process, carried out under controlled atmosphere, and high-purity conditions, in a homemade Czochralski furnace properly designed for fluoride single crystals. The pulling rate during the growth was 1 mm/h with a 7 r/min rotation rate.

The measured room temperature absorption coefficient and emission spectra of 1% Ho:YLF crystal associated with the transitions between the ground-state ($^5I_8$) and the first excited-state ($^5I_7$) Stark manifolds are shown in Fig. 1(b). The shaded area in the absorption spectrum is the so-called "cooling tail" with $\lambda > \lambda_f$, where $\lambda_f = c/\nu_f \sim 2015$ nm denotes the mean fluorescence wavelength. To quantify the sample's EQE and α_b, and to investigate whether the sample is of "cooling grade," a mid-IR laser source of modest power (1–2 W), narrow linewidth (<1 nm), and tunable in the vicinity of λ_f is required. For this purpose, we designed and constructed a singly resonant continuous-wave (CW) optical parametric oscillator (OPO) based on temperature-tuned periodically polled lithium niobate (PPLN) [23,24]. This OPO, pumped by a high-power CW fiber laser at 1070 nm, can be tuned from 1900 nm to 2300 nm, and is further detailed in the Methods section.

The cooling efficiency η_c of the Ho:YLF sample is evaluated at room temperature by measuring the temperature change (ΔT) induced by irradiating the sample with the OPO output, as the wavelength is tuned from below to above λ_f. Under steady-state condition and for small temperature changes, $\Delta T(\lambda) = K\eta_c(\lambda)P_{\text{abs}}(\lambda)$, where P_{abs} is the absorbed laser (OPO) power, and K is a constant (scaling factor) that varies inversely with the thermal load on the sample. Therefore,

$\eta_c(\lambda) = \Delta T/KP_{abs}$ can be extracted by measuring ΔT and the absorbed power as a function of λ. The aforementioned method is termed laser-induced thermal modulation spectroscopy (LITMoS) [25]. Figure 2(a) shows the schematic of a typical LITMoS experiment in which the cooling sample is positioned on top of two transparent low thermal conductivity holders inside a vacuum chamber (10^{-6} Torr, 1 Torr = 133.322 Pa) in order to minimize the conductive and convective thermal loads and thus maximize ΔT induced by a double pass of the OPO beam through the sample. This is particularly useful at enhancing the signal-to-noise ratio in the long wavelength regime, where the absorption coefficient (and hence P_{abs}) drops drastically. The relative temperature change ΔT of the sample is measured with an IR thermal camera (Thermal Eye Nanocore 640 L3-Communications Corporation, Texas), which views the sample from outside the vacuum chamber through a KCl window.

The temperature change of the crystal at each wavelength is extracted from thermal images following standard image processing that involves spatial and temporal averaging. Care is taken to ensure that the thermal camera response is linear (i.e., by keeping the temperature change of the sample to $|\Delta T| < 3$ K) using ~0.5–1 W of input power, and that the ambient temperature remains constant during the experiment. The absorbed power $P_{abs}(\lambda)$ at each excitation wavelength λ is calculated from the measured room-temperature absorption coefficient using the Beer–Lambert law. The normalized data $\Delta T(\lambda)/KP_{abs}(\lambda)$ are then fitted with Eq. (1) by adjusting K, η_{ext}, and α_b. Note that, for simplicity, we assume α_b does not vary with wavelength within the narrow (~200 nm) spectral range of interest. This assumption is adopted primarily because the origin of the parasitic absorption is not precisely known from sample to sample, as, e.g., it could arise from a variety of transition metals or other RE ions [19].

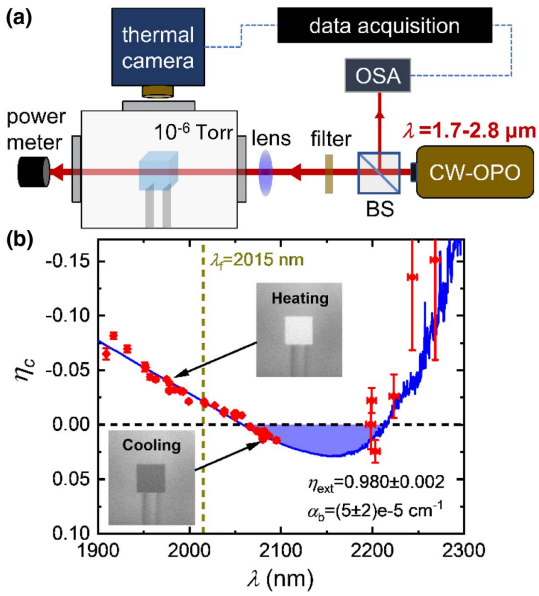

Fig. 2. (a) Schematic of mid-IR laser cooling and LITMoS test setup for Ho-doped crystals. (b) LITMoS test result for 1% Ho:YLF crystal; the theoretical fit to the data, using Eq. (1), gives the external quantum efficiency (η_{ext}) and the parasitic (background) absorption coefficient (α_b). The insets show two thermal images corresponding to heating and cooling regimes.

It is further assumed that α_b is also temperature independent. The validity of both these assumptions and their implication in cryocooling experiments will be revisited later in this paper.

The measured LITMoS test on the 1% Ho:YLF sample at room temperature ($T = 300$ K) along with its corresponding fitting parameters α_b and η_{ext} are shown in Fig. 2(b). A net-cooling window is observed between $\lambda_{c1} = 2059$ nm and $\lambda_{c2} = 2215$ nm. Generally, in high-purity samples where $\alpha_b < 10^{-3}$ cm^{-1}, η_{ext} can be estimated with a fair degree of accuracy from λ_f/λ_{c1}, while the value of α_b is highly sensitive to the location of λ_{c2}. The best fit to data, as shown in Fig. 2(b), gives $\eta_{ext} = 98.0\% \pm 0.2\%$ and $\alpha_b = (5 \pm 2) \times 10^{-5}$ cm^{-1} for this 1% Ho:YLF sample.

3. RESULTS: LOW-TEMPERATURE ANALYSIS

Thus far, we have demonstrated that this Ho:YLF sample is of cooling grade at room temperature, exhibiting maximum cooling at a wavelength of $\lambda = 2150$ nm. The next task at hand is to identify its potential for cryocooling operation by evaluating its MAT. This in turn necessitates evaluation of $\eta_c(\lambda, T)$ down to cryogenic temperatures. As stated earlier, starting with the assumptions that η_{ext} and α_b are temperature independent, we need to obtain the temperature dependence of only the remaining ingredients of η_c, namely, $\alpha_r(\lambda, T)$ and $\lambda_f(T)$. The latter is measured by recording the fluorescence spectra $S(\lambda)$ associated with the first excited-state transition as the temperature of the sample, placed in a cryostat, is varied from 300 K to 80 K. The emission spectra are collected by a fiber-coupled mid-IR optical spectrum analyzer (Thorlabs OSA203B). Since YLF is an anisotropic (uniaxial) crystal, the spectra for both π ($E\|c$) and σ ($E\perp c$) polarizations are separately recorded at each temperature by using appropriate polarizers in front of the collection fiber. The mean fluorescence wavelength $\lambda_f^{\pi,\sigma}(T) = \int \lambda S^{\pi,\sigma}(\lambda, T)\mathrm{d}\lambda / \int S^{\pi,\sigma}(\lambda, T)\mathrm{d}\lambda$ is calculated for each polarization followed by evaluating the exiting total mean fluorescence wavelength by performing a weighted average along the three Cartesian axes of the crystal—given by $\lambda_f(T) = (2/3)\lambda_f^{\sigma}(T) + (1/3)\lambda_f^{\pi}(T)$.

The remaining task is now to determine the temperature-dependent resonant absorption coefficients $\alpha_r(\lambda, T)$ by utilizing the reciprocity theorem [26,27] and the McCumber relation, which gives $\alpha_r(\lambda, T) \propto \lambda^5 S(\lambda, T) e^{hc/\lambda kT}$. Proportional spectra thus calculated are then calibrated to a directly measured absorption value (e.g., at $\lambda = 2055$ nm) to get the exact absorption spectra $\alpha_r(\lambda, T)$ at each temperature. The absorption spectra obtained by reciprocity agree well with those directly measured with a Fourier transform infrared (FTIR) spectrometer, while having the advantage of exhibiting less noise in the long wavelength ($\lambda > 2065$ nm) tail, which is of particular interest for laser cooling.

Figure 3(a) shows the measured temperature variation of λ_f for the 1% Ho:YLF crystal. The data are normalized to room-temperature value $\lambda_f^{Ho}(300\ \mathrm{K}) = 2015$ nm for comparison with the same measured quantity for a cooling grade 1% Tm:YLF crystal [23,28] having $\lambda_f^{Tm}(300\ \mathrm{K}) = 1822$ nm. A red shift of ~1% is seen in Ho:YLF compared to ~3.5% in Tm:YLF as the temperature is varied from 300 K to 80 K. As stated earlier, this signifies the narrower width of the

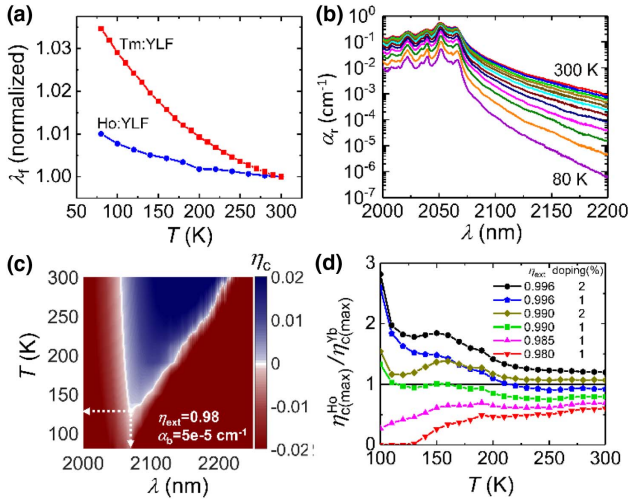

Fig. 3. (a) Temperature dependence of the mean fluorescence wavelength (λ_f) for cooling grade 1% Ho:YLF and 1% Tm:YLF crystals. For comparison, data are normalized to room temperature values. (b) Temperature dependence of the resonant absorption coefficient of the $^5I_8$–$^5I_7$ transition in 1% Ho:YLF from 300 K to 80 K in 20 K steps ($E\|c$). (c) Cooling efficiency $\eta_c(\lambda, T)$ versus excitation wavelength and crystal temperature. The blue and red regions correspond to the cooling ($\eta_c > 0$) and heating ($\eta_c < 0$) regimes, respectively, with the white transition line indicating the local minimum achievable temperature (MAT) at a given wavelength. The global MAT (as indicated by dashed lines) is $\sim 130 \pm 10$ K at $\lambda = 2070 \pm 0.5$ nm, which corresponds to the $E_{12} \rightarrow E_{13}$ transition in Ho^{3+} (Ref. [21]). (d) Ratio of maximum cooling efficiency of the Ho:YLF sample over the optimal 10% Yb:YLF sample assuming various η_{ext} and doping concentrations for Ho:YLF.

excited-state manifold in Ho, which makes it highly suitable for cryogenic cooling. Additionally, a nearly two-fold enhancement in the absorption cross section of Ho^{3+} over Tm^{3+} makes the case of Ho-based cryocoolers in mid-IR even stronger [21]. The calibrated absorption spectra for $E\|c$ obtained from the reciprocity relation in the same temperature range are given in Fig. 3(b). This polarization was chosen, as Ho:YLF exhibits a larger absorption cross section for $E\|c$ at wavelengths in the cooling tail.

With η_{ext}, α_b, $\lambda_f(T)$, and $\alpha_r(\lambda, T)$ known, we plot $\eta_c(\lambda, T)$ to identify the cooling and heating spectral regimes at all temperatures, and subsequently obtain the value of MAT for this crystal. Figure 3(c) shows the map of η_c versus T and λ. The white demarcation in this plot signifies $\eta_c = 0$ and marks the MAT for the corresponding excitation wavelength. The lowest (or global) MAT for this crystal is $\sim 130 \pm 10$ K at $\lambda \sim 2070$ nm, which corresponds to the $E_{12} \rightarrow E_{13}$ transition between $^5I_8$ and $^5I_7$ manifolds [Fig. 1(a)] in Ho:YLF crystal.

It is also worth noting that this wavelength conveniently coincides with readily available high-power Tm- and Ho-fiber lasers [29,30]. Additionally, Tm-fiber (or disk) lasers, when pumped by high-power diodes near 790 nm, are known to be highly efficient (~65%) due to the well-known 2-for-1 cross-relaxation pumping scheme [31–33].

While future efforts must focus on lowering the MAT beyond 130 K, we should recall that this value of MAT was estimated following the assumption that α_b was independent of temperature. However, recent experiments in Yb:YLF crystals have revealed that this assumption must be revisited; these crystals have been cooled to lower temperatures than predicted by the constant α_b models [11,18]. In particular, α_b in a 5% doped Yb:YLF sample was shown to reduce by nearly an order of magnitude as the temperature was lowered from 300 K to 100 K, which in turn lowered MAT from about 110 K to below 90 K, in excellent agreement with experimental results [11,18]. Such temperature dependence in α_b cannot be generalized, since the parasitic absorption can arise from a variety of contaminants; however, it is not unreasonable to reassess the MAT in Ho:YLF assuming a similar dependence. For example, lowering α_b to 1×10^{-5} cm^{-1} further reduces the MAT to about 100 K for the current Ho-doped sample. As the absorption efficiency depends on α_b/α_r, even further improvement in MAT can be achieved by increasing the doping concentration. Investigations on excited-state dynamics of Ho^{3+} ions in ZBLAN glass [34] show that concentration quenching of the radiative decay from the $^5I_7$ manifold sets in only at ~4% doping. However, theoretical studies have suggested that higher doping concentrations may potentially increase the nonradiative decay due to energy transfer up-conversion (ETU) process in Ho^{3+} ions [35,36]. Further experiments are needed (and are currently underway) to investigate the role of higher Ho concentrations on the EQE and laser cooling performance.

4. DISCUSSION

We have demonstrated optical refrigeration in a Ho-doped material in the mid-IR for the first time. This offers multiple potential advantages over existing Yb-doped systems for cryogenic cooling as well as for realization of high-power mid-IR radiation balanced lasers.

Optical refrigeration, since its first demonstration, has been touted as a mechanism for realizing all-solid-state cryocoolers without any moving parts or vibrations. Such a device was recently demonstrated by cooling an IR sensor to <135 K by using Yb:YLF as the cooling element [12]. An essential requirement for a practical optical cooler is that the load or cold finger must be efficiently shielded from the intense fluorescence emanating from the cooling crystal using a delicately designed thermal link [12]. The next generation of Yb-based cryocoolers is to be integrated with the NIST single-crystal Si reference cavities that need to be cooled to 124 K in a totally vibration-free environment [37,38]. A mid-IR-based optical refrigerator can be highly beneficial for this application, since the load (Si cavity) is transparent to the ~2 μm fluorescence, and therefore the thermal link can be eliminated altogether.

As described by Eq. (1) and the ensuing discussion, mid-IR optical refrigeration can potentially offer enhanced cooling efficiency due to energy scaling and other characteristic advantages of the system. The current material with 1% doping and $\eta_{ext} \sim 98\%$ does not yet match the cooling efficiency of our best Yb:YLF system with 10% doping concentration and $\eta_{ext} > 99\%$. However, Ho-doped crystals having a narrower ground-state manifold, higher absorption cross section, and lower parasitic background absorption promise to outperform Yb:YLF. A modest improvement in η_{ext} would allow the $E_{12} \rightarrow E_{13}$ resonance in Ho:YLF occurring at ~2065 nm to be

accessed, thus leading to considerable cooling efficiency enhancement. This can be achieved through high-purity growth of Ho:YLF crystals or using other host materials with lower phonon energies such as BaY_2F_8 (BYF), which could further suppress the multi-phonon relaxation mechanism. Recent studies on Tm-doped crystals show that BYF [24,28] with a phonon energy of 350 cm^{-1} (i.e., 100 cm^{-1} lower than in YLF) [39] improves η_{ext} from 0.980 to >0.995. Moreover, a reasonable and modest increase in the dopant concentration [34] would further enhance the cooling efficiency above that of Yb-doped systems. To illustrate this, we have evaluated the maximum cooling efficiency of Ho-doped crystal $\eta_{c(max)}^{Ho}$—subject to minor modifications—relative to the efficiency $\eta_{c(max)}^{Yb}$ for the best Yb-doped system (10% Yb:YLF, $\eta_{ext} = 0.996$) [10]. The ratio of these cooling efficiencies versus crystal temperature down to 100 K is shown in Fig. 3(d). We have kept the background absorption coefficient α_b in both crystals the same as their measured room temperature values. We note that if η_{ext} in 1% Ho:YLF (or BYF) was to improve from 0.98 to 0.99, it would already match the performance of the 10% Yb:YLF at low temperatures of interest (e.g., 150 K). Combined with the availability of higher-efficiency mid-IR lasers at the optimum cooling wavelength (e.g., Tm-fiber lasers), this promises an enhanced wall-plug efficiency. Moreover, increasing the doping concentration to 2% can lead to a two-fold efficiency enhancement of Ho- over Yb-doped systems at 150 K (i.e., 0.24% over 0.13%). The enhancement in the cooling efficiency ratio seen at lower temperatures is a consequence of Yb:YLF approaching its MAT ($\eta_c = 0$) at a higher temperature than Ho, assuming improved doping and quantum efficiency. As discussed earlier, recent experiments suggest a strong reduction in the background absorption at low temperatures, which in turn will lead to lower MATs for these materials [18]. In short, the confluence of lower energy gap, narrower ground- and excited-state manifolds, higher absorption cross section, and lower parasitic absorption makes Ho-doped crystals potentially superior to Yb-doped systems for cryogenic optical refrigeration with reasonable improvements in material synthesis.

A different yet promising application of anti-Stokes fluorescence cooling is more concerned with the removal of heat rather than cooling to low temperatures. This process is particularly attractive in lasers where the laser action and cooling correspond to the same atomic transition [40]. The principle of such "athermal" lasers was proposed by Bowman [41] and was termed "radiation balanced lasers" (RBLs). RBL operation was soon demonstrated in Yb:YAG rods with CW powers approaching 500 W and free from any thermal distortion at 1050 nm [42]. Identifying high-quality cooling-grade materials in mid-IR, as reported in this paper, paves the way for realization of high-power eye-safe RBLs at 2 μm [24,28,43,44]. A mid-IR RBL may be realized by pumping at $\lambda_P = 2070$ nm with laser operation at $\lambda_L \sim 2090$ nm. Improving η_{ext} and the doping concentration not only enhances the cooling efficiency for refrigeration applications, as previously discussed, but equally improves the optical-to-optical efficiency and maximum power density that can be extracted from such a laser under radiation-balanced operation.

In summary, we demonstrated net optical refrigeration in a Ho-doped material for the first time. EQE ($\eta_{ext} = 98\%$), parasitic background absorption ($\alpha_b = 5 \times 10^{-5}$ cm^{-1}), and temperature-dependent emission and absorption spectra were carefully measured for a 1% Ho:YLF crystal. Subsequently, the cooling efficiency as a function of wavelength and temperature was evaluated, which in turn led to an estimation of the MAT of 130 ± 10 K at ~2070 nm. We conclude that Ho:YLF is superior to Tm-doped crystals for mid-IR cryocooler applications due to narrower energy manifolds, availability of high-power lasers, and larger absorption cross section at the optimum cooling wavelength. Furthermore, we showed that with these spectral characteristics, Ho-doped crystals may outperform Yb-doped systems, assuming reasonable improvements in doping and quantum efficiency. Finally, the utility of Ho for high-power, mid-IR, eye-safe RBLs was discussed.

5. METHODS

A mid-IR CW OPO is designed and constructed to serve as the tunable pump source for optical refrigeration in Ho:YLF. The nonlinear crystal is an $L = 50$ mm long temperature-tuned MgO-doped PPLN (MgO:PPLN) crystal with multiple gratings that provide quasi-phase matching (QPM). The pump laser is a CW Yb:fiber laser at 1070 nm (IPG, YLR-500-SM).

The OPO cavity is a singly resonant standing-wave V-cavity [Fig. 4(a)] formed by two concave mirrors (M1 and M2) having radius of curvature ROC = −20 cm, and a flat output coupler (OC). The OPO operates in singly resonant mode with M1 and M2 having broadband high reflectance in the signal range (1.7–2.1 μm) and high transmission for both pump (1070 nm) and the idler (2.2–2.8 μm). The signal is coupled out from OC with ~4% transmission. Since our pump laser at 1070 nm has a relatively broad linewidth (≳1 nm), resonating the signal (instead of the idler) makes it possible to improve the pump acceptance bandwidth to 1 nm [45]. The pump laser is focused to a waist size of $w_0 \sim 70$ μm at the middle of the PPLN; this corresponds to $L/2z_0 \sim 2.3$, where z_0 is the Rayleigh range. A pair of intracavity etalons (300 μm thick UV fused silica and 500 μm thick ZnSe) is inserted to reduce the linewidth of the OPO to <0.5 nm. The tuning curve of the OPO versus PPLN

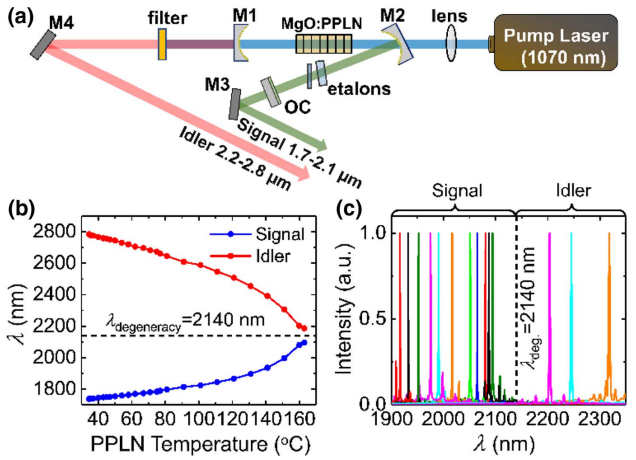

Fig. 4. (a) Schematic of the CW-OPO design for mid-IR optical refrigeration in Tm- and Ho-doped crystals. (b) Phase-matching curve of the mid-IR CW-OPO. (c) Typical normalized narrow linewidth signal and idler spectra of the CW-OPO.

temperature is shown in Fig. 4(b) for a grating period $\Lambda = 31.9$ μm. Figure 4(c) shows the corresponding normalized spectra of the narrow linewidth signal and idler indicating the tuning range used for optical refrigeration of the 1% Ho:YLF crystal.

Funding. Air Force Office of Scientific Research (AFOSR) (FA9550-15-1-0241, FA9550-16-1-0362); U.S. Army (W911SR-17-C-0039).

Acknowledgment. We thank Drs. Arlete Cassanho and Hans P. Jenssen (AC Materials Inc., Tarpon Springs, FL) for growing high-purity Ho:YLF crystals. We also thank Dr. Richard Epstein (ThermoDynamic Films LLC), Dr. Zhou Yang (UNM), and Dr. Brian Walsh (NASA) for useful discussions. The authors declare that there are no conflicts of interest related to this paper.

REFERENCES

1. P. Pringsheim, "Zwei bemerkungen über den unterschied von lumineszenz- und temperaturstrahlung," Z. Phys. **57**, 739–746 (1929).
2. M. Sheik-Bahae and R. I. Epstein, "Optical refrigeration," Nat. Photonics **1**, 693–699 (2007).
3. A. Kastler, "Quelques suggestions concernant la production optique et la détection optique d'une inégalité de population des niveaux de quantifigation spatiale des atomes. Application à l'expérience de Stern et Gerlach et à la résonance magnétique," J. Phys. Radium **11**, 255–265 (1950).
4. R. I. Epstein, M. I. Buchwald, B. C. Edwards, T. R. Gosnell, and C. E. Mungan, "Observation of laser-induced fluorescent cooling of a solid," Nature **377**, 500–503 (1995).
5. J. Fernandez, A. J. Garcia-Adeva, and R. Balda, "Anti-Stokes laser cooling in bulk erbium-doped materials," Phys. Rev. Lett. **97**, 033001 (2006).
6. N. J. Condon, S. R. Bowman, S. P. O'Connor, R. S. Quimby, and C. E. Mungan, "Optical cooling in Er^{3+}:KPb_2Cl_5," Opt. Express **17**, 5466–5472 (2009).
7. B. Zhong, J. Yin, Y. Jia, L. Chen, Y. Hang, and J. Yin, "Laser cooling of Yb^{3+}-doped $LuLiF_4$ crystal," Opt. Lett. **39**, 2747–2750 (2014).
8. A. Volpi, G. Cittadino, A. Di Lieto, and M. Tonelli, "Anti-Stokes cooling of Yb-doped KYF_4 single crystals," J. Lumin. **203**, 670–675 (2018).
9. D. V. Seletskiy, S. Melgaard, M. Sheik-Bahae, S. Bigotta, A. DiLieto, and M. Tonelli, "Laser cooling of a semiconductor load using a Yb:YLF optical refrigerator," Proc. SPIE **7614**, 761409 (2010).
10. S. D. Melgaard, A. R. Albrecht, M. P. Hehlen, and M. Sheik-Bahae, "Solid-state optical refrigeration to sub-100 Kelvin regime," Sci. Rep. **6**, 20380 (2016).
11. A. Gragossian, J. Meng, M. Ghasemkhani, A. R. Albrecht, and M. Sheik-Bahae, "Astigmatic Herriott cell for optical refrigeration," Opt. Eng. **56**, 011110 (2016).
12. M. P. Hehlen, J. Meng, A. R. Albrecht, E. R. Lee, A. Gragossian, S. P. Love, C. E. Hamilton, R. I. Epstein, and M. Sheik-Bahae, "First demonstration of an all-solid-state optical cryocooler," Light Sci. Appl. **7**, 15 (2018).
13. D. V. Seletskiy, R. Epstein, and M. Sheik-Bahae, "Laser cooling in solids: advances and prospects," Rep. Prog. Phys. **79**, 096401 (2016).
14. M. Sheik-Bahae and R. I. Epstein, "Laser cooling of solids," Laser Photon. Rev. **3**, 67–84 (2009).
15. C. W. Hoyt, M. Sheik-Bahae, R. I. Epstein, B. C. Edwards, and J. E. Anderson, "Observation of anti-Stokes fluorescence cooling in thulium-doped glass," Phys. Rev. Lett. **85**, 3600–3603 (2000).
16. W. Patterson, S. Bigotta, M. Sheik-Bahae, D. Parisi, M. Tonelli, and R. Epstein, "Anti-Stokes luminescence cooling of Tm^{3+} doped BaY_2F_8," Opt. Express **16**, 1704–1710 (2008).
17. E. E. Brown, U. Hömmerich, E. Kumi-Barimah, A. Bluiett, and S. B. Trivedi, "Comparative spectroscopic studies of Ho:KPb_2Cl_5, Ho:KPb_2Br_5, and Ho:YAG for 2 μm laser cooling applications," Proc. SPIE **9380**, 93800O (2015).
18. A. Gragossian, A. Volpi, J. Meng, A. R. Albrecht, S. Rostami, M. P. Hehlen, and M. Sheik-Bahae, "Investigation of temperature dependence of quantum efficiency and parasitic absorption in rare-earth doped crystals," Proc. SPIE **10550**, 1055006 (2018).
19. S. Melgaard, D. Seletskiy, V. Polyak, Y. Asmerom, and M. Sheik-Bahae, "Identification of parasitic losses in Yb:YLF and prospects for optical refrigeration down to 80 K," Opt. Express **22**, 7756–7764 (2014).
20. P. W. France, S. F. Carter, and J. M. Parker, "Oxidation states of 3D transition metals in ZrF_4 glasses," Phys. Chem. Glasses **27**, 32–41 (1986).
21. B. M. Walsh, "Spectroscopy and excitation dynamics of the trivalent lanthanides Tm^{3+} and Ho^{3+} in $LiYF_4$," NASA Contractor Report 4689 (1995).
22. A. Sugiyama, M. Katsurayama, Y. Anzai, and T. Tsuboi, "Spectroscopic properties of Yb doped YLF grown by a vertical Bridgman method," J. Alloys Compd. **408–412**, 780–783 (2006).
23. S. Rostami, A. R. Albercht, M. R. Ghasemkhani, S. D. Melgaard, A. Gragossian, M. Tonelli, and M. Sheik-Bahae, "Optical refrigeration of Tm:YLF and Ho:YLF crystals," Proc. SPIE **9765**, 97650P (2016).
24. S. Rostami, A. R. Albrecht, M. Tonelli, and M. Sheik-Bahae, "Advances in laser cooling of Tm:YLF crystals," Proc. SPIE **10121**, 1012101 (2017).
25. S. D. Melgaard, "Cryogenic optical refrigeration: laser cooling of solids below 123 K," Ph.D. thesis (University of New Mexico, 2013).
26. D. E. McCumber, "Einstein relations connecting broadband emission and absorption spectra," Phys. Rev. **136**, A954–A957 (1964).
27. F. Cornacchia, A. Toncelli, and M. Tonelli, "2 μm lasers with fluoride crystals: research and development," Prog. Quantum Electron. **33**, 61–109 (2009).
28. S. Rostami, Z. Yang, A. R. Albrecht, A. Gragossian, M. Peysokhan, M. Ghasemkhani, A. Volpi, M. Tonelli, and M. Sheik-Bahae, "Advances in mid-IR solid-state optical cooling and radiation-balanced lasers," Proc. SPIE **10550**, 105500Q (2018).
29. K. Yin, B. Zhang, G. Xue, L. Li, and J. Hou, "High-power all-fiber wavelength-tunable thulium doped fiber laser at 2 μm," Opt. Express **22**, 19947–19952 (2014).
30. N. Simakov, Z. Li, Y. Jung, J. M. O. Daniel, P. Barua, P. C. Shardlow, S. Liang, J. K. Sahu, A. Hemming, W. A. Clarkson, S.-U. Alam, and D. J. Richardson, "High gain holmium-doped fibre amplifiers," Opt. Express **24**, 13946–13956 (2016).
31. W. A. Clarkson, L. Pearson, Z. Zhang, J. W. Kim, D. Shen, A. J. Boyland, J. K. Sahu, and M. Ibsen, "High power thulium doped fiber lasers," in *Optical Fiber Communication Conference and National Fiber Optic Engineers Conference*, OSA Technical Digest (Optical Society of America, 2009), paper OWT1.
32. D. J. Richardson, J. Nilsson, and W. A. Clarkson, "High power fiber lasers: current status and future perspectives [Invited]," J. Opt. Soc. Am. B **27**, B63–B92 (2010).
33. B. Anderson, A. Flores, J. Grosek, and I. Dajani, "High power Tm-doped all-fiber amplifier at 2130 nm," in *Conference on Lasers and Electro-Optics*, OSA Technical Digest (Optical Society of America, 2017), paper SM1L.3.
34. A. F. H. Librantz, S. D. Jackson, F. H. Jagosich, L. Gomes, G. Poirier, S. J. L. Ribeiro, and Y. Messaddeq, "Excited state dynamics of the Ho^{3+} ions in holmium singly doped and holmium, praseodymium-codoped fluoride glasses," J. Appl. Phys. **101**, 123111 (2007).
35. G.-Z. Dong and X.-L. Zhang, "Role of upconversion in optical refrigeration: a theoretical study of laser cooling with Ho^{3+} doped fluoride crystals," J. Opt. Soc. Am. B **30**, 3041–3047 (2013).
36. G.-Z. Dong, X.-L. Zhang, and L. Li, "Energy transfer enhanced laser cooling in Ho^{3+} and Tm^{3+}-codoped lithium yttrium fluoride," J. Opt. Soc. Am. B **30**, 939–944 (2013).
37. T. Kessler, C. Hagemann, C. Grebing, T. Legero, U. Sterr, F. Riehle, M. J. Martin, L. Chen, and J. Ye, "A sub-40-mHz-linewidth laser based on a silicon single-crystal optical cavity," Nat. Photonics **6**, 687–692 (2012).
38. O. Graydon, "Payload success," Nat. Photonics **12**, 315 (2018).

39. M. P. Hehlen, M. Sheik-Bahae, and R. I. Epstein, "Solid-state optical refrigeration," in *Handbook on the Physics and Chemistry of Rare Earths* (2014), Vol. **45**, pp. 179–260.
40. G. Nemova, *Laser Cooling: Fundamental Properties and Applications* (Pan Stanford, 2017).
41. S. R. Bowman, "Lasers without internal heat generation," IEEE J. Quantum Electron. **35**, 115–122 (1999).
42. S. R. Bowman, S. O. Connor, S. Biswal, and N. J. Condon, "Demonstration and analysis of a high power radiation balanced laser," in *CLEO 2011—Laser Science to Photonic Applications* (2011), paper CMH4.
43. S. Rostami, A. R. Albrecht, A. Volpi, M. P. Hehlen, M. Tonelli, and M. Sheik-Bahae, "Tm-doped crystals for mid-IR optical cryocoolers and radiation balanced lasers," arXiv:1901.07737 (2019).
44. G. Nemova and R. Kashyap, "Radiation-balanced amplifier with two pumps and a single system of ions," J. Opt. Soc. Am. B **28**, 2191–2194 (2011).
45. J. Powers and P. Haus, *Fundamentals of Nonlinear Optics*, 2nd ed. (CRC Press, 2017).